Q. J. R. Meteorol. Soc. (2002), **128**, pp. 1–20

A minimal axi-symmetric tropical cyclone model

By Nguyen Chi Mai*

Centre for Dynamical Meteorology and Oceanography, Monash University, Australia

By Roger K. Smith†, Hongyan Zhu and Wolfgang Ulrich

Meteorological Institute, University of Munich

May 8, 2002

Abstract

Solutions of an axisymmetric version of the minimal three-dimensional numerical model of a tropical cyclone developed by Zhu *et al.* are described and compared with those of the three-dimensional model. Vortex evolution is similar in the two models during the early stages of intensification, but the period of rapid intensification occurs earlier in the axisymmetric model due to the higher effective resolution obtained using a staggered grid. There are marked differences at later times, when, in the three-dimensional model, asymmetric structures develop. The findings are compared with those of an earlier study by Anthes.

The axisymmetric model is used to investigate certain fundamental aspects of tropical-cyclone dynamics, including the emergence of a region of supergradient winds in the boundary layer and the evolution of regions satisfying necessary conditions for inertial and barotropic instability. Supergradient winds develop in the boundary layer within a radius of about 100 km of the vortex axis at an early stage of evolution and appear to be a natural feature of the vortex boundary layer. The development of flow regions satisfying necessary conditions for inertial and barotropic instability occur later and may be attributed *inter alia* to the upward transfer of air with relatively high angular momentum from the boundary layer to the middle and upper layers by the secondary circulation of the vortex and the downward transfer of air with relatively low angular momentum to the middle layer. A linear analysis of a two-layer slab-symmetric flow suggests why inertial instability does not occur in the axisymmetric model. Barotropic instability does not appear to be the mechanism responsible for the growth of asymmetries in the calculations using the three-dimensional version of the model.

1. Introduction

The development of numerical models for tropical cyclones began in earnest towards the end of the sixties with pioneering studies by Yamasaki (1968a,b,c), Ooyama (1969), Rosenthal (1969, 1970, 1971), Sundqvist (1970), and Anthes *et al.* (1971a,b). Because of limited computer resources at that time, these early models were axisymmetric, but some had significant vertical resolution: Sundqvist's model had 10 layers and Yamasaki's (1968c) model had 13 layers. While the methods used to represent moist processes have come under some scrutiny in recent times (Smith, 2000), many basic features of tropical cyclone dynamics were elucidated by these studies. An early milestone was the development of asymmetric models (Anthes *et al.*, 1970a,b), which despite their limitations of resolution and domain size, provided fundamental insights into a range of basic processes involved in

* Present affiliation: National Center for Hydro-Meteorological Forecasting, Hanoi, Vietnam

† Corresponding author address: Prof. Roger K. Smith, Meteorological Institute, University of Munich, Theresienstr. 37, 80333 Munich, Germany, Email: roger@meteo.physik.uni-muenchen.de

tropical cyclone evolution including the growth of asymmetries, the development of supergradient winds in the surface boundary layer, and the natural development of flow regions that might be unstable to one or more types of dynamic instability. To our knowledge, calculations exploring these features have not since been repeated, at least with models that include moist processes.

During the last three decades, numerical models have improved significantly as a result of improved numerical algorithms together with improvements in our understanding of, and the representation of, physical processes. Furthermore, computing hardware has developed dramatically to the point that it is now possible to run high resolution models with sophisticated representations of physical processes, both for forecasting and research purposes. Nevertheless, there continues to be a role for simple models for developing basic understanding. Most of the models that fall into this category make the assumption of axial symmetry, such as those of Wada (1979), DeMaria and Pickle (1988), and Emanuel (1986, 1989, 1995, 1997), although extensions of Ooyama's (1969) model to three-dimensional flow configurations have been used to study tropical cyclone motion (e.g. Shapiro, 1992; Dengler and Reeder, 1997; Dengler, 1998; Dengler and Smith, 1998) and the role of asymmetries in vortex spin-up (Shapiro, 2000). Most of these models have a minimal vertical resolution also: Emanuel's models have effectively two layers and the others three, except for Wada's model, which has four. A limitation of many of the models is the closure for deep convection, which, except in Emanuel's and Wada's models, is based upon the convergence of moist static energy in the boundary layer. While this closure may be adequate for the mature tropical cyclone, it may be poor for much of the intensification stage (see e.g. Smith, 2000).

In a recent paper, Zhu *et al.* (2001, henceforth ZSU) used a minimal three-dimensional model with a fully-integrated representation of moist physics to explore the evolution of tropical cyclones for different representations of deep cumulus convection. The model removes some of the limitations of the Ooyama-type models and can be regarded as an extension (albeit a nontrivial one) of Emanuel's 1989 model to three-dimensions, but for maximum simplicity it still has only three vertical layers. The present study compares an axisymmetric version of the ZSU model with the three-dimensional version and goes on to use the former to investigate aspects of cyclone dynamics for which it is especially suitable.

One reason why corresponding calculations with an axisymmetric model are called for is that, in the three-dimensional calculations, an initially symmetric vortex on an f-plane develops flow asymmetries, which become important features after a certain time. The growth of asymmetries may be expected in all three-dimensional models that use a square grid to represent a circular vortex, and while their presence is not unphysical, their initiation in the model is unphysical. Comparisons between the three-dimensional and axisymmetric versions of the model can help to assess the importance of the asymmetries on the evolution of tropical cyclones. Even so, as indicated above, tropical cyclone models reported in the literature tend to have been either axisymmetric or three dimensional and as far as we are aware, the study by Anthes *et al.* (1971b) is the only one in which calculations of axisymmetric and three-dimensional versions of ostensibly[‡] the same model have been compared.

Because of the fundamental nature of the processes studied by Anthes *et al.* (1971b) and Anthes (1972), and because of the many limitations of their models as touched upon above, we were motivated to repeat and extend some of their calculations using the present model and its three-dimensional counterpart. The latter models incorporate many improvements and refinements compared with those used by Anthes and coworkers: in particular

[‡] In fact, there were some differences in numerical formulation of the two versions, a staggered grid being used in the axisymmetric case, giving this version a higher effective resolution.

they have higher horizontal resolution, a much larger domain and an improved representation of convective processes. The precise differences are detailed in section 4.

There are certain basic problems for which the axisymmetric model is more suited to investigate. One important problem studied here is the development of supergradient winds in the boundary layer, which lead to the occurrence of the maximum wind speed within the boundary layer, rather than above it. This is an unusual feature of boundary layers in general and appears to be special to the termination boundary layer of an intense vortex. While the problem is not new, it seems to have received relatively little attention in the literature. Anthes (1972) discussed the phenomenon briefly, but didn't investigate it in detail. Shapiro (1983) found a region of supergradient winds in the inner core of an axisymmetric vortex boundary layer, within the radius of maximum tangential wind speed above the layer, but the main focus of his study was the steady asymmetric boundary layer beneath a translating hurricane. Recently, Kepert and Wang (2001) presented high-resolution numerical solutions of the tropical-cyclone boundary layer in a model with an imposed steady pressure gradient above the layer. They found a strong radial jet in the core region in which the tangential wind speed was 10 - 25% supergradient. In the present study we investigate the evolution of the boundary layer flow in an axisymmetric vortex model driven by buoyancy forces associated with moist convection. In particular we examine the stage and radii at which supergradient winds emerge. Time-radius plots of various quantities are used to provide a more complete picture of vortex evolution than radial profile plots at a few selected times as are often presented. A companion paper (Smith, 2002) explores a simple slab boundary layer model for a steady axisymmetric hurricane.

Another problem that has received little attention in the literature since Anthes' (1972) study is the development of regions of symmetric inertial instability and barotropic instability within a tropical cyclone. Some of the early papers investigated the possible role of inertial instability on tropical-cyclone evolution and concluded that the effect was unlikely to be important, at least in models with very limited vertical resolution (see e.g. Ooyama, 1969, section 4; Anthes, 1972, section 3f). Anthes (1972) explained the reasons for expecting the development of such regions, but showed only the time-variation of minima in the azimuthal averages of the relevant stability parameters. Ooyama (1987) explored a simple model for the outflow layer in a hurricane and found that although the forced outflow generates areas of negative absolute vorticity, it was not possible to simulate oscillatory or unstable flow patterns that could be identified as a manifestation of inertial instability. Other approaches to the stability problem have focussed on the instability of steady, hurricane-like, tangential wind profiles (Flatau and Stevens, 1989; Weber and Smith, 1994; Schubert *et al.*, 1999; Kossin *et al.*, 2001). In particular, Kossin *et al.* (2001) used a barotropic model to investigate the instability of vortices with a secondary wind maximum. Here we use the axisymmetric model to examine the evolution of flow regions satisfying the necessary conditions for inertial and barotropic instability, including the natural tendency for vortices to develop a secondary wind maximum. However, it appears that barotropic instability is an unlikely mechanism for explaining the asymmetries that develop in the calculations using the three-dimensional version of the model.

In the next section we describe briefly the model formulation and in section 3 the cumulus parameterization schemes. The numerical model experiments we carry out are detailed in section 4 and the results are presented in section 5. A summary and conclusions are contained in section 6.

2. Description of the model

(a) *Governing equations*

The model is based on the hydrostatic primitive equations in cylindrical sigma-coordinates (r, λ, σ) on an f-plane, where

$$\sigma = \frac{p - p_{top}}{p_s - p_{top}} = \frac{p - p_{top}}{p^*}, \tag{1}$$

$p^* = p_s - p_{top}$ and p_{top} are the surface and top pressures, and p_{top} is a constant, taken here to be 100 mb. Then the upper and lower boundary conditions require that $\dot{\sigma} = 0$ at $\sigma = 0$ and $\sigma = 1$, where $\dot{\sigma} = D\sigma/Dt$ is the vertical σ-velocity, t is the time, and D/Dt is the material derivative. The zonal and meridional momentum equations and the hydrostatic equation are:

$$\frac{\partial u}{\partial t} = -u\frac{\partial u}{\partial r} - \dot{\sigma}\frac{\partial u}{\partial \sigma} + fv + \frac{v^2}{r} + \frac{R\theta\sigma(p^*\sigma + p_{top})^{\kappa-1}}{p_o^{\kappa}}\frac{\partial p^*}{\partial r} - \frac{\partial \phi}{\partial r} + D_u, \tag{2}$$

$$\frac{\partial v}{\partial t} = -u\frac{\partial v}{\partial r} - \dot{\sigma}\frac{\partial v}{\partial \sigma} - fu - \frac{uv}{r} + D_v \tag{3}$$

$$\frac{\partial \phi}{\partial \sigma} = -\frac{Rp^*(p^*\sigma + p_{top})^{\kappa}}{p_o^{\kappa}}\theta \tag{4}$$

where u and v are velocity components in the radial $r-$ and tangential λ-directions, f is the Coriolis parameter, evaluated here at 20°N, R is the specific gas constant for dry air, $\kappa = R/c_p$, c_p is the specific heat of dry air, θ is the potential temperature, ϕ is the geopotential, and D_u and D_v represent the frictional drag in the $r-$ and λ-directions, respectively. The specification of D_u and D_v is described by ZSU. The surface pressure tendency equation, derived from the continuity equation and boundary conditions is

$$\frac{\partial p*}{\partial t} = -\int_0^1 \frac{1}{r}\frac{\partial}{\partial r}(p^* r u)d\sigma \tag{5}$$

and $\dot{\sigma}$ is given by

$$\dot{\sigma} = -\frac{1}{p^*}\int_0^{\sigma} \frac{1}{r}\frac{\partial}{\partial r}(p^* r u)d\sigma + \frac{\sigma}{p^*}\int_0^1 \frac{1}{r}\frac{\partial}{\partial r}(p^* r u)d\sigma \tag{6}$$

The thermodynamic and moisture equations are

$$\frac{\partial \theta}{\partial t} = -u\frac{\partial \theta}{\partial r} - \dot{\sigma}\frac{\partial \theta}{\partial \sigma} + Q_\theta \tag{7}$$

and

$$\frac{\partial q}{\partial t} = -u\frac{\partial q}{\partial r} - \dot{\sigma}\frac{\partial q}{\partial \sigma} + Q_q \tag{8}$$

where θ is the potential temperature, q is specific humidity, Q_θ and Q_q represent the diabatic heat and moisture sources, respectively, including those associated with deep cumulus convection. The temperature T is related to θ by

$$T = \left(\frac{p}{p_o}\right)^{\kappa}\theta = \frac{(p^*\sigma + p_{top})^{\kappa}}{p_o^{\kappa}}\theta \tag{9}$$

where $p_o = 1000$ mb.

(*b*) *Explicit moist processes*

Explicit condensation is treated in the simplest possible way. If at any time the air becomes saturated at a grid point, grid-scale condensation and precipitation processes are allowed. The excess water vapour is condensed to liquid water and is assumed to precipitate out while the latent heat released is added to the air. This procedure is applied before the sub-grid-scale convection scheme, whereupon the convection scheme is applied to a conditionally-unstable atmosphere with relative humidity less than 100% (n.b. if the relative humidity equals 100%, the condition for convective instability is not satisfied).

(*c*) *Radiative cooling and surface turbulent fluxes*

Newtonian cooling is added in the thermodynamic equation to represent the effect of radiative cooling and the turbulent flux of momentum to the sea surface and the fluxes of sensible heat and water vapour from the surface are represented by bulk aerodynamic formulae as described in ZSU.

(*d*) *Boundary and initial conditions*

The calculations are carried out in a cylindrical domain ($0 \leq r \leq R,\ \ 0 \leq \sigma \leq 1$) with the following boundary conditions:

$$u = 0, \quad v = 0, \quad \frac{\partial A}{\partial r} = 0, \quad at \quad r = 0 \tag{10}$$

$$u = 0, \quad v = 0, \quad \frac{\partial A}{\partial r} = 0, \quad at \quad r = R \tag{11}$$

where A can be any of the quantities u, v, θ, q. The initial axisymmetric vortex is barotropic and the tangential velocity distribution is detailed in ZSU. It has a maximum wind speed of 15 m s^{-1} at a radius of 120 km.

The surface pressure and geopotential are obtained by integrating the gradient wind equation in σ-coordinates radially inwards, i.e.

$$RT_s[\ln(p_s(R)) - \ln(p_s(r))] = \int_r^R \left(fV_s + \frac{V_s^2}{r}\right) dr. \tag{12}$$

$$\phi(R) - \phi(r) = \int_r^R \left(fV + \frac{V^2}{r} - \frac{RT}{p}\sigma\frac{\partial p*}{\partial r}\right) dr \tag{13}$$

The determination of the surface pressure using Eq. (12) requires the surface temperature to be known. Here it is taken to be the sea surface temperature. The temperature in each layer is obtained from the potential temperature, obtained by solving Eq. (9).

The far-field temperature and humidity structure are based on the mean West Indies sounding for the 'hurricane season' (Jordan, 1957), but the near-surface mixing ratio has been reduced slightly so that the sounding is initially stable to deep convection. The initial surface pressure is 1015 mb. In the presence of the initial vortex, the minimum surface pressure (at the vortex centre) is 1008 mb. Horizontal variations of mixing ratio in the presence of the initial vortex are neglected. Details of the initial sounding are given in ZSU.

(*e*) *The numerical method*

The model is divided vertically into three unequally deep layers with boundaries at

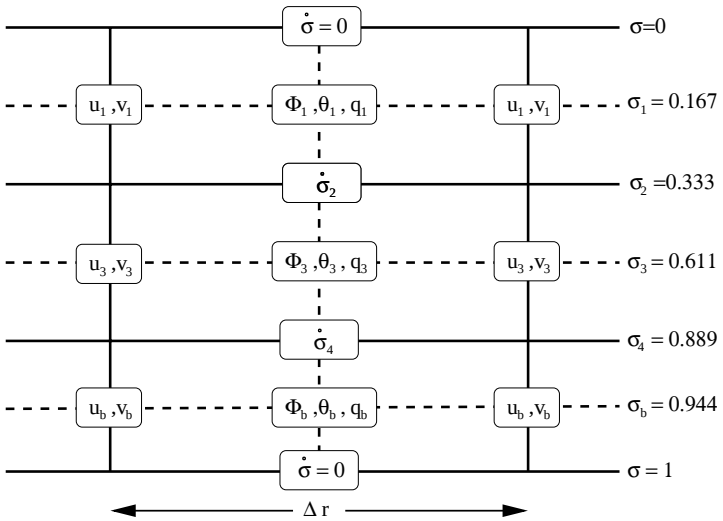

Figure 1. Configuration of σ-levels in the model showing locations where the dependent variables are stored. The horizontal velocity components, geopotential, potential temperature, specific humidity and the moist static energy used in the convection scheme (see section 3) are calculated at levels 1, 3 and b and the vertical velocity $\dot{\sigma}$ and convective mass flux are stored at levels 2 and 4.

$\sigma = 1$, σ_4, σ_2 and 0 (see Fig. 1). All the dependent variables, such as horizontal velocity, potential temperature, specific humidity and geopotential, are defined in the middle of each layer ($\sigma = \sigma_b$, σ_1, and σ_3), and the vertical velocity is staggered, i.e. it is defined at the boundaries between layers. The variables are staggered in the radial direction also as indicated in Fig. 1. The equations are expressed in finite difference form in both the horizontal and vertical and integrated using the Adams-Bashforth third-order method. The initial pressure, temperature, mixing ratio and geopotential height in the middle of each layer and at the boundaries between layers are listed in Table A1 of ZSU.

(*f*) *Subgrid-scale diffusion*

An important consideration in tropical cyclone modelling is the suppression of small-scale noise and numerical instability in the calculations. This problem becomes of extreme importance when the formulation provides for the explicit release of latent heat. The methods used in this paper are detailed in an appendix.

3. Cumulus parameterization schemes

There are options in the model for using three different representations of subgrid-scale cumulus convection as detailed in section 3 of ZSU. Here we use only one of these schemes, a version of the scheme proposed by Arakawa (1969) modified to include the effects of precipitation-cooled downdraughts.

4. The numerical experiments

In the next section we describe the results of two numerical experiments. Experiment 1 uses the Arakawa representation of sub-grid-scale deep convection and allows for grid-scale latent heat release as described in section 3b. We take this to be the control experiment.

Experiments 2 is similar to Expt. 1, but does not have any representation of subgrid-scale convection. The results of these experiments are compared in section 5(a) with the corresponding three-dimensional calculations of ZSU. Experiment 1 is used in the sections 5(b) - 5(c) to investigate particular aspects of vortex dynamics.

5. Results

(*a*) *Comparison of calculations from the axisymmetric and three-dimensional models*

Figure 2 compares time series of the maximum boundary-layer wind speed and minimum surface pressure in Expts. 1 and 2 with those for the corresponding three-dimensional calculations of ZSU. The time series of wind speed show both the maximum point value (labelled 3) and the azimuthally-averaged maximum value (dashed line) for the three-dimensional calculations. All calculations are carried out with a horizontal grid spacing of 20 km. In general, the pattern of vortex intensification is similar in the two- and three-dimensional calculations with a gestation period, a period of rapid growth, and a mature stage in which the vortex strength fluctuates about some relatively high mean value. In the calculation with the Arakawa closure, the intensification rate during the gestation period is a little larger in the axisymmetric calculation and the gestation period is shorter. This behaviour is like that described in a similar comparison by Anthes *et al.* (1971) and it is reasonable to attribute it to the higher effective resolution provided by the staggered grid in the axisymmetric model. Anthes *et al.* (1971) showed, *inter alia*, that the pressure gradient term is represented more accurately on a horizontally-staggered grid and that this accounts for the stronger vortex. Unfortunately, it is difficult to properly compare the differences in the results of our study with theirs because there are substantial differences between the two model formulations. Although their model has three layers also, they define $\sigma = p/p_s$ so that the ratio of layer depths is different from ours; they use also a much smaller domain size, less than one quarter of the 2000 km radius domain used here; a larger initial vortex; and a coarser grid (30 km compared with 20 km used here). They use also a different staggering of variables in the vertical, with the geopotential stored at the same levels as the vertical σ-velocity. Further, their model uses a parameterization scheme based on moisture convergence and does not have an explicit water cycle.

After the period of rapid intensification, the maximum intensity as measured by the maximum tangential wind speed is comparable in the two and three-dimensional calculations with the latter showing larger amplitude fluctuations. The minimum surface pressure is, in general, higher in the three-dimensional calculations, a feature that is true of both experiments. We attribute this fact to the evolution of asymmetries as discussed below.

The behaviour of the calculations in the case with only an explicit representation of latent heat release is broadly in line with that for the Arakawa closure, but there is little difference in the decay rate between the axisymmetric and three-dimensional calculations during the gestation period as would be expected.

The higher effective resolution provided by the staggered grid in the axisymmetric calculation is evident in Fig. 3, which compares time series of the maximum boundary-layer wind speed and minimum surface pressure in Expt. 1 with those for the corresponding three-dimensional calculation, but with a horizontal grid spacing of 10 km. The time series in the two calculations are closer to each other for the first 36 h of integration than in Fig. 2a and b, because the gestation period in the three-dimensional calculation is reduced. However, there are major differences in the time series at later times when the vortex in the three-dimensional calculation develops asymmetries. We examine these asymmetries in more depth in subsection (e) below.

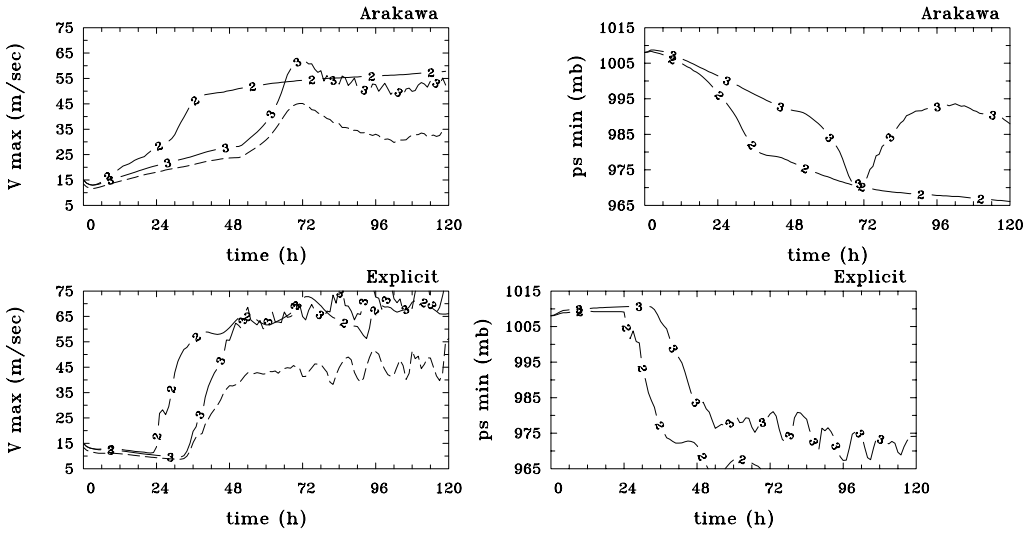

Figure 2. Comparison between time series of the maximum boundary-layer wind speed (left panels) and the minimum surface pressure (right panels) for Expts. 1 and 2 (labelled 2) and the corresponding time series for the azimuthally-averaged wind field (dashed curves) and maximum point value wind speed (labelled 3) in three-dimensional calculations of ZSU. Upper panels are for the Arakawa closure (Expt. 1) and lower panels for the case with only the explicit release of latent heat (Expt. 2).

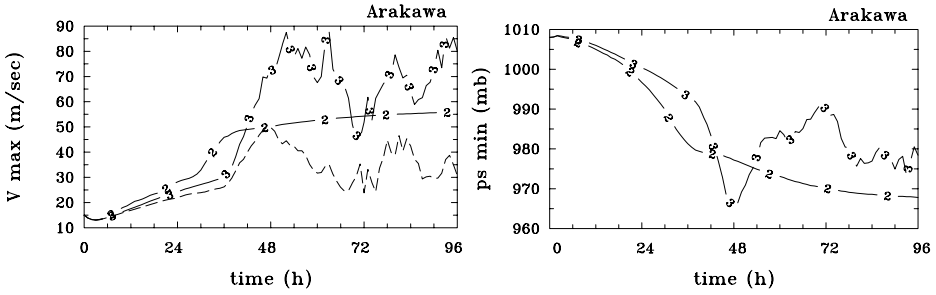

Figure 3. As for Fig. 2, but for the Arakawa closure and with 10 km horizontal grid spacing in the three-dimensional case and 20 km spacing in the two-dimensional case.

(*b*) *Development of supergradient winds in the boundary layer*

The frictionally-induced inflow in the tropical-cyclone boundary layer is a prominent feature of the cyclone structure and can be attributed to the disruption of approximate gradient-wind balance above the boundary layer by turbulent stresses (see e.g. Smith, 1968). According to boundary layer theory (e.g. Jones and Watson, 1963), the perturbation pressure gradient normal to the boundary is negligibly small so that the horizontal pressure gradient is approximately constant through the boundary layer, equal to that just above the layer. However, the tangential wind speed is reduced by friction within the boundary layer with a consequent reduction of the centrifugal and Coriolis forces. The result is a net inwards pressure gradient force in the boundary layer and it is this that drives the inflow. Based on this view of boundary layer dynamics, it is surprising to find that the maximum tangential wind speed actually occurs in the boundary layer instead of the layer above. This feature may be seen in the time-radius isotach plots of the difference between the tangential wind speed in the middle layer and the boundary layer, $v_3 - v_b$, for the control experiment, shown in the left panel of Fig. 4. It is notable that after about 6 h, a region

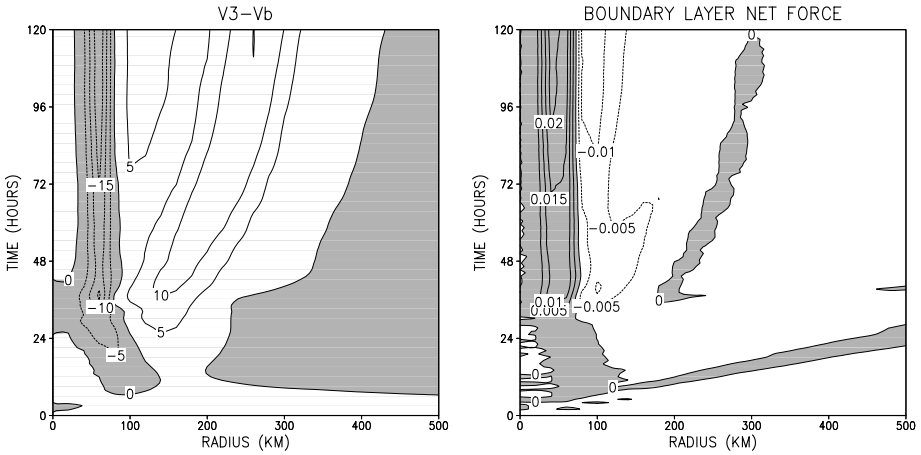

Figure 4. Time-radius plots of isotachs of $v_3 - v_b$ (left panel, contour interval 5 ms^{-1}, negative values shaded), and the net pressure gradient force (pressure gradient minus centrifugal and Coriolis force) per unit mass in the boundary layer for Expt. 1 (right panel, contour interval 5 $\times 10^{-3}$ ms^{-2}, positive values shaded).

develops surrounding the vortex axis in which the tangential wind speed in the boundary layer exceeds that in the overlying vortex. There are two possible interpretations of this result. On the one hand it might be argued that boundary layer theory cannot be applied within the context of the present model, because of the coarse vertical resolution. More precisely, boundary layer theory relates to the radial pressure gradient at the top of the boundary layer, whereas the pressure gradient at the next model level is characteristic of a height several kilometres above the boundary layer. On the other hand, if boundary layer theory *is* valid in the inner core region, the boundary layer winds there might still become supergradient in the sense that the sum of the centrifugal and Coriolis forces exceeds the inwards-directed radial pressure gradient. In fact, time-radius plots of the net radial force (excluding friction) in the boundary layer (right panel of Fig. 4), indicate that this is the case and that the region of negative net force in this layer contains the region of negative $v_3 - v_b$.

Reasons to expect the occurrence of supergradient winds in the boundary layer are discussed by Anthes (1974, p506). As explained by Ooyama (1982), the spin-up of a symmetric* vortex requires inflow to occur above the boundary layer and the only conceivable mechanism for producing convergence in this region is the production of buoyancy in the inner-core region of an immature vortex (see e.g. Smith, 2000). As rings of air converge in this region, they approximately conserve their absolute angular momentum so that the tangential wind speed at a particular radius and particular time is related to the parcel's initial absolute angular momentum and the radial displacement that it experiences. In contrast, air parcels converging in the boundary layer lose a fraction of their absolute angular momentum as a result of surface friction, but they undergo much larger inward displacements. This difference in displacements is confirmed by Fig. 5, which shows the radial trajectories of air columns in the two layers as the vortex evolves. The calculations in the right panel of Fig. 4 imply that the frictional loss of angular momentum *is* outweighed by the larger inward displacement in the inner core region as the vortex intensifies.

The occurrence of wind speeds that are larger in the boundary layer than outside

* There exists also an asymmetric mechanism that can lead to vortex intensification as described in recent papers by Möller and Montgomery (2000) and refs. and Shapiro (2000).

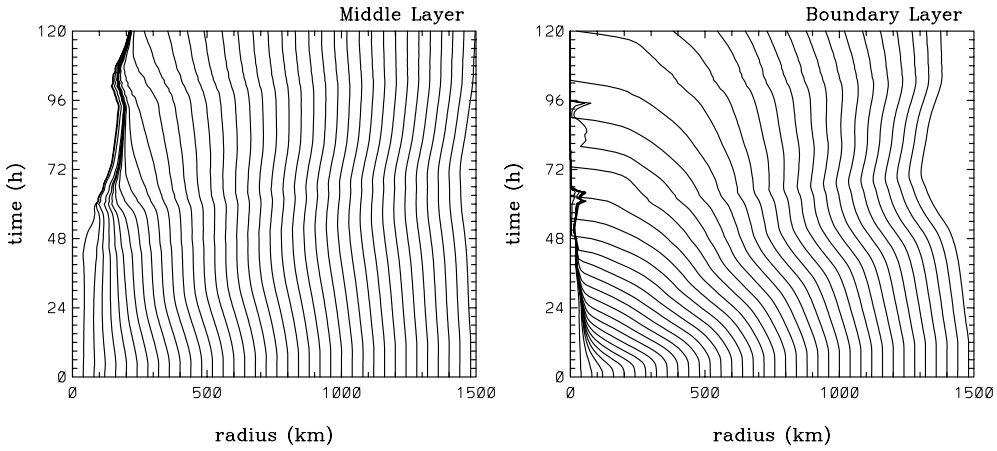

Figure 5. Time-radius plots showing the trajectory of air columns in the middle layer (left panel) and (b) the boundary layer (right panel) in Expt. 1.

it is unusual in fluid flows in general and may be special to the terminating boundary layers of intense vortices. The development of such a region has important consequences for tropical cyclones (and possibly also tornados, waterspouts and dust devils) as it provides a reason to expect that the highest wind speeds in these vortices will be found close to the surface. Also, the rapid deceleration of the boundary layer inflow in tropical cyclones must be an important limiting factor on both the smallness of the "eye" and on the ultimate vortex intensity. This seems to be an aspect of tropical-cyclone structure that has received less attention than it deserves. A recent study of the tropical-cyclone boundary layer by Kepert (2001) has shown that the vertical advection of supergradient winds can lead to strong outflow jets at the top of the boundary layer, a feature that may be associated with vortex breakdown (an excellent review of vortex breakdown in the context of tornadoes is given by Snow, 1982; 959-961). The study by Smith (2002) shows that the region of supergradient winds in a slab boundary-layer model may be accompanied by significant oscillations of vertical velocity at the top of the boundary layer. However, the radial scale of these oscillations is below the resolution of the present model.

(*c*) *Development of possibly unstable flow regions*

Another aspect of tropical-cyclone dynamics that arguably has received less attention in the literature than it deserves is the development of regions where necessary criteria for inertial instability and/or barotropic instability are satisfied, especially in the upper troposphere. In an axisymmetric model, the criterion for inertial instability is that the quantity $I^2 = \zeta_{abs}(f + 2V/r) < 0$, where $V(r)$ is the tangential wind speed at radius r and $\zeta_{abs} = f + \zeta$ is the vertical component of absolute vorticity (Rayleigh, 1916). If $V(r) > -\frac{1}{2}rf$, regions of negative I^2 coincide with those of negative ζ_{abs}. Regions of negative I^2 are potentially important; for one thing instability may occur there and for another, the occurrence of these regions precludes the existence of a balanced solution. Ooyama (1969, p10) noted the development of such regions in his balanced three-layer hurricane model, but argued that the instability does not occur because of the coarse vertical resolution. The necessary condition for barotropic instability is that the radial gradient of absolute vorticity changes sign at some radius (see e.g. Anthes, 1972). While barotropic instability cannot be realized in an axisymmetric model, since unstable disturbances have azimuthal structure, it may occur in the three-dimensional model. We investigate this possibility in

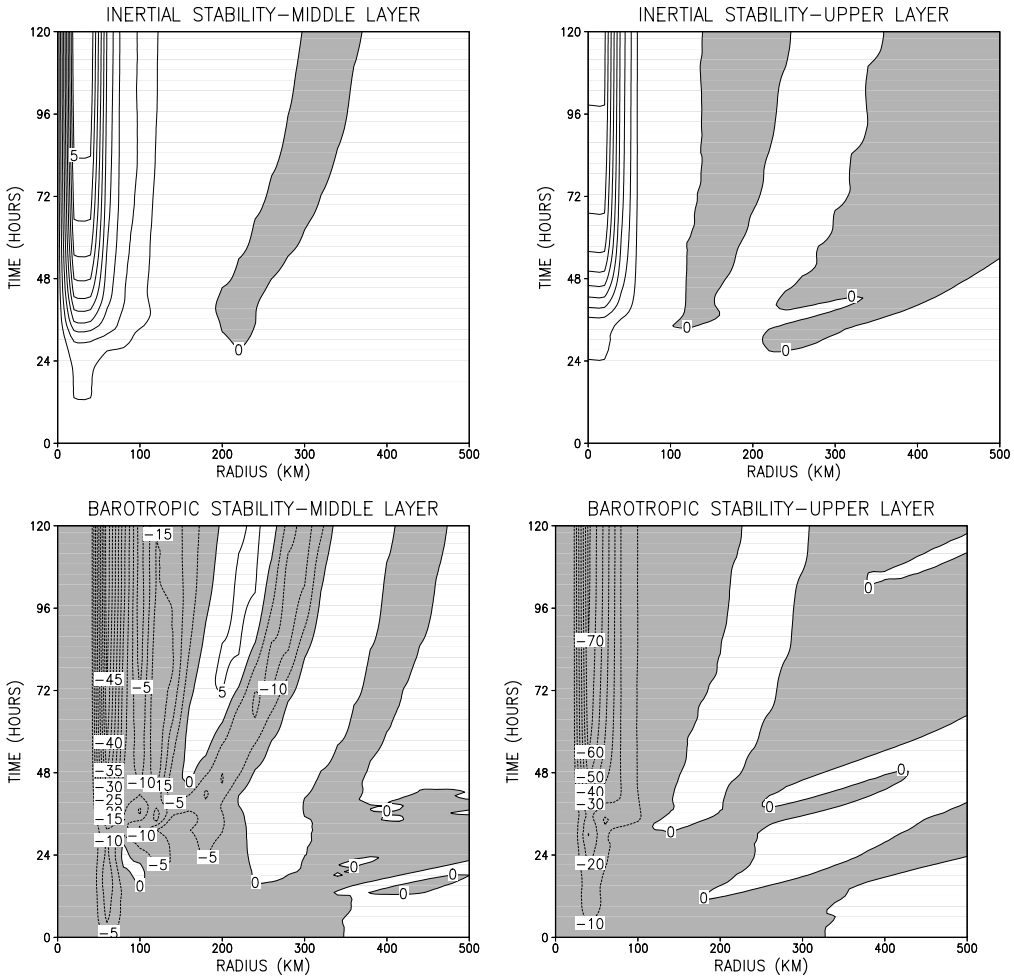

Figure 6. Upper panels: time-radius plots of the inertial stability parameter, I^2, for Expt. 1 in the middle layer (left), and the upper layer (right). Contour intervals are 5 $\times 10^{-7}$ s^{-2} and 1 $\times 10^{-6}$ s^{-2}, respectively. Negative values are shaded. Lower panels show the corresponding plots of the radial gradient of relative vorticity, $\partial\zeta/\partial r$. A necessary condition for barotropic instability is that this quantity changes sign at some radius. Contour intervals are 5 $\times 10^{-9}$ s^{-2} and 1 $\times 10^{-8}$ s^{-2}, respectively. Negative values are shaded.

subsection (f) below.

(*d*) *Inertial instability*

The upper panels of Fig. 6 show time-radius cross sections of I^2 for Expt. 1 in the middle and upper layers, respectively. A region where $I^2 < 0$ develops in both layers a little after a day and a second region develops in the upper layer a few hours later. In the middle layer, the region of negative I^2 is confined to radii between about 180 km and 370 km and moves gradually outwards with time. In the upper layer the overall region of instability is much more widespread. The occurrence of multiple regions of negative I^2 was noted also by Anthes (1972; see p471), but he showed profiles of this quantity only at selected times (his Fig. 13) and only in the upper layer.

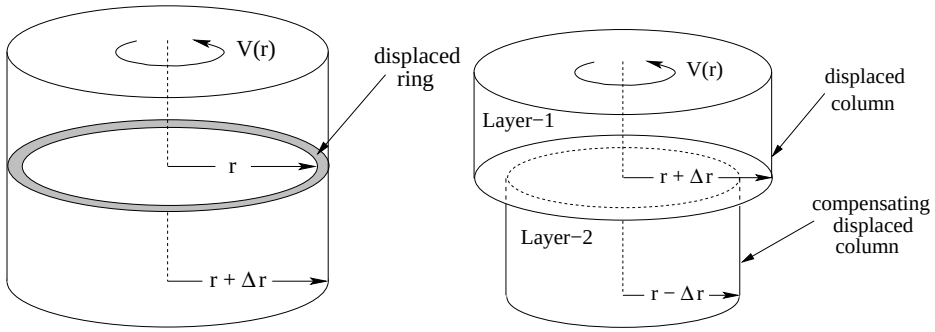

Figure 7. Schematic diagram illustrating the idea of inertial instability in a continuous fluid (left panel), and in a two-layer fluid system (right panel). See text for discussion.

The ideas relating to inertial instability may be illustrated by reference to Fig. 7. The left panel depicts the radial displacement of a thin annular tube of fluid in a background flow that is rotating with tangential velocity distribution $V(r)$ about a vertical axis. This velocity field is assumed to be in gradient wind balance. If the tube is displaced from radius r to radius $r + \Delta r$ while conserving its absolute angular momentum, and if it experiences the existing local pressure gradient at its new radius, it will be subjected to a net outward force, approximately equal to $-I^2\Delta r$. If $I^2 > 0$, the force is a restoring force and the displacement is stable. In contrast, if $I^2 < 0$, the force is in the direction of the displacement and leads to instability.

The foregoing argument breaks down if it is not possible to displace a tube of fluid relative to its neighbours at different heights, but at the same radius. Then there can be no difference in force with height and no instability *within* the layer. Clearly the tube argument is inapplicable to a barotropic flow, but in a two-layer fluid, an outward displacement in one layer may be compensated by an inward displacement in the other on account of continuity (see Fig. 7, right panel). If as a result of such displacements, the force experienced by displaced ring-like columns of fluid is in the direction of the displacement, the secondary circulation will strengthen and in doing so will extract kinetic energy from the basic state vortex. Although tube arguments are inappropriate in this situation, a stability analysis is revealing. Such an analysis for the simplest case of slab-symmetric geometry is described in an appendix. The analysis shows that the appropriate criterion is based on a suitably weighted mean value of I^2, say $\overline{I}^2$, and that only waves of horizontal wavelength larger than a certain threshold are unstable. Therefore if the horizontal extent of the region over which $\overline{I}^2$ is negative is less than this wavelength, instability will not occur. Calculations show that $\overline{I}^2$ is dominated by the contribution from the middle layer (Fig. 6, upper left panel). Equation (A.7) in the appendix shows that the threshold wavelength for instability decreases with decreasing density contrast (i.e. static stability), whereupon *in a multi-layer or continuous system, waves of higher vertical wavenumber will have a greater chance of being unstable at a given horizontal scale.*

The development of regions with $I^2 < 0$ (or $\zeta_{abs} < 0$) in tropical cyclones is associated with the secondary circulation of the vortex and may be interpreted variously in terms of the vorticity equation; or in terms of the vertical transfer of absolute angular momentum, M_{abs}, by this circulation (Anthes, 1972, pp471-472); or in terms of the vertical transfer of potential vorticity (Flatau and Stevens, 1987) by the circulation. For example, Anthes notes that in the early stages of cyclone development, M_{abs} increases radially outwards.

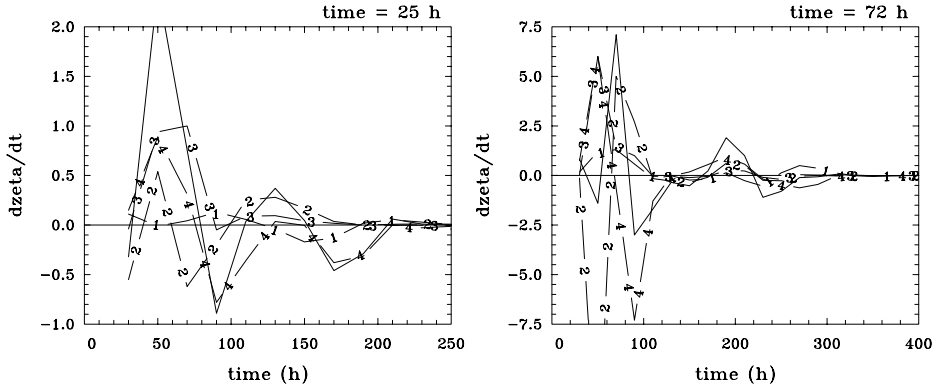

Figure 8. Radial profiles of contributions to the vorticity tendency in Eq. 14 at 25 h (left panel) and 72 h (right panel). The integer labels 1-4 denote the contributions from horizontal advection, divergence, vertical advection and tilting, respectively. The solid line is the sum of these contributions. The units are 1.0×10^{-10} s^{-2}. Note the different scales on the two plots.

However, the reversal of the radial gradient of M_{abs} (corresponding with the production of negative ζ_{abs}) occurs when air at large radii (large M_{abs}) is advected inwards in the boundary layer. When this air is ultimately carried upwards in the inner core region and outwards aloft, it may retain a higher value of M_{abs} than air at the same level, but at a larger radial distance from the vortex axis, despite some frictional loss of M_{abs} to the sea surface. These arguments are related to those for the development of supergradient winds in the boundary layer as discussed in subsection (b).

We explore briefly the vorticity approach using our model, focussing on the vorticity tendency for layer 3, which contributes most to the mean inertial stability parameter $\bar{I}^2$. The accuracy of such diagnostics is limited by the the minimal vertical resolution of the model, but is best for layer 3. The vorticity equation may be written in σ-coordinates as

$$\frac{\partial \zeta}{\partial t} = -u\frac{\partial}{\partial r}(\zeta + f) - \dot{\sigma}\frac{\partial \zeta}{\partial \sigma} - \frac{\zeta + f}{r}\frac{\partial ru}{\partial r} - \xi\frac{\partial \dot{\sigma}}{\partial r} + \frac{1}{r}\frac{\partial rD_v}{\partial r} \tag{14}$$

where $\xi = \partial v/\partial\sigma$ is the horizontal component of relative vorticity in these coordinates and $\zeta = (1/r)\partial(rv)/\partial r$ is the vertical component. Figure 8 shows plots of the first four terms on the right-hand-side of this equation for layer 3 as functions of radius at the two times: $t = 25$ h and $t = 72$ h. In the finite difference form of the equation, the twisting term (fourth on the rhs) involves an average of four separate contributions from staggered points at levels 2 and 4. The vertical advection term (second on the rhs) was estimated using the finite difference form of the expression $-\partial(\dot{\sigma}\zeta)/\partial\sigma + \zeta\partial\dot{\sigma}/\partial\sigma$. At 25 h, just prior to the emergence of the region of negative I^2 in the upper left panel of Fig. 6, the vorticity tendency is negative in this region, the major contribution being from the tilting term (curve labelled 4). It turns out that most of this contribution, itself, is from the tilting of radial vorticity component by the radial gradient of vertical velocity at the upper level (level 2), which is negative. At 72 h, typical of conditions in the mature stage of evolution, all four terms make comparable contributions to the negative tendency in the vorticity equation at radii where the negative absolute vorticity occurs in the upper left panel of Fig. 6.

(*e*) *Barotropic instability*

The lower panels of Fig. 6 show time-radius cross sections of $\partial\zeta/\partial r$ for Expt. 1 in the middle and upper layers. At the initial instant the radial vorticity gradient is negative in

both layers inside a radius of about 320 km and it is positive beyond this radius. As time proceeds, the region of positive gradient moves to radii larger than 500 km after about a day, but three other regions develop in the middle layer and two in the upper layer, the region of strongest positive gradient being in a radial band between about 150 km and 270 km from the axis in the middle layer (see lower left panel).

Reasons for the development of new vortex profiles satisfying the necessary conditions for barotropic instability are suggested by the calculations of vortex intensification by Schubert and Alworth (1987; see their Fig. 4). These authors examined the evolution of potential vorticity in a symmetric, balanced hurricane-like vortex associated with an imposed heat source surrounding the vortex core. During the early stages of development, a potential vorticity minimum in the upper level of the cyclone is located at the vortex centre, above a potential vorticity maximum. Subsequently, the potential vorticity minimum is pushed off the centre by the ascending high potential vorticity air, thus creating a region where the potential vorticity gradient changes sign on an isentropic surface. As noted by Flatau and Stevens (1989), this development can set the stage for barotropic instability. Slightly more realistic calculations were carried out by Möller and Smith (1994), but the essential features of the potential vorticity evolution were confirmed (see their Fig. 3). The development of profiles with new sign changes in the relative vorticity gradient in our model may be attributed to the development of new extrema in the vorticity profile itself, as discussed in subsection (d) above. This interpretation is consistent with the foregoing discussion in terms of potential vorticity.

(*f*) *The growth of asymmetries*

During the rapid deepening period, the vortices in the three-dimensional calculations develop marked asymmetries in the inner core region as described by ZSU (see section 5c and Fig. 10). These are reflected in the large differences between the maximum azimuthally-averaged wind speed and the maximum point-value wind speed in these calculations shown in Fig. 2. Generally, the axisymmetric calculations yield a higher wind speed than the azimuthally-averaged wind speed in the three-dimensional calculations. The reasons for this difference, and indeed, the reasons for the differences in the time series of maximum boundary-layer wind speed and minimum surface pressure between the axisymmetric and three-dimensional calculations is evident by examining the pattern of asymmetries that develop in the latter calculations. In the calculation shown by ZSU (see Fig. 10 therein), the asymmetry in relative vorticity and vertical motion in the middle troposphere is dominated by an azimuthal wavenumber-4 pattern during the gestation period, and a marked wavenumber-2 structure evolves during the period of rapid intensification. ZSU suggested that the initiation of wavenumber-4 pattern is associated with the representation of an axisymmetric flow on a square grid and the wavenumber-2 pattern with the use of channel boundary conditions in a domain of finite (albeit relatively large) size. We examine these possibilities further here.

In Expt. 1, a weak azimuthal wavenumber-4 asymmetry in the vorticity field is evident also from an early stage in the calculation. This asymmetry does not rotate. After 60 h of integration, an azimuthal wavenumber-2 vorticity asymmetry rapidly appears in the inner core region (within 200 km of the axis). The two cyclonic portions of this asymmetry form vorticity centres of comparable strength that rotate around each other and subsequently merge. These centres have corresponding low pressure minima and are associated with enhanced vertical motion aloft (figures not shown). Assuming local gradient wind balance, the smaller scale of the individual vortices would imply a higher central pressure for the same maximum tangential wind speed (see e.g. Callaghan and Smith, 1998). Asymmetries occur also in the calculation with the Emanuel and Ooyama closures for deep convection,

and in the case with only the explicit release of latent heat (see ZSU, Fig. 10), but in each case their structure (e.g. the dominant azimuthal wavenumber) is different.

The suggestion that the wavenumber-2 component is a result of using channel boundary conditions must now be dismissed. We carried out two additional calculations: one with a larger domain size (6000 km × 6000 km, instead of 4000 km × 4000 km) and the other with box boundary conditions, with zero normal flow at the boundary. In both cases there was no detectable change in the evolution of the wavenumber-2 pattern. The asymmetry is also insensitive to the diffusivity. We carried out one calculation with twice the amount of damping. The extra smoothing delayed the onset of rapid intensification by about 12 h, but the wavenumber-2 asymmetry is still a prominent feature when rapid intensification occurs.

The axisymmetric model was developed, *inter alia*, to serve as a benchmark for understanding the role of the asymmetries on vortex evolution. The calculations in subsection (e) indicate that barotropic instability could be involved in the growth of some of the asymmetric components, although the higher effective resolution in the axisymmetric case means that there are quantitative differences in the axisymmetric and three-dimensional calculations as evidenced by the plots in Fig. 2. In fact, the azimuthally-averaged tangential wind speed in the three-dimensional calculation (with 20 km horizontal resolution) does not show the development of a secondary wind maximum in the middle layer. Even so, the initial tangential wind profile in both calculations is such that the radial vorticity gradient changes sign and as such satisfies a necessary condition for barotropic instability.

A linear stability analysis of the initial tangential wind profile using the method described by Weber and Smith (1994) shows that it is, in fact, barotropically unstable to a disturbances of azimuthal wavenumber-2, although the e-folding time scale of this mode is relatively long, on the order of 66 h. Nevertheless, the profile is barotropically stable to higher wavenumbers, in particular to wavenumber-4, which is the first asymmetric component to appear in the ZSU calculations. As the vortex profile changes only slowly during the gestation period, it is unlikely that it becomes barotropically unstable to wavenumber-4 during this period.

During the period of rapid development, the tangential wind profile changes rapidly and the vortex becomes baroclinic, strengthening at low levels and weakening aloft. Indeed, the radius at which the radial vorticity gradient in the middle layer changes sign moves outwards after about 14 h, and shortly afterwards a further region of positive vorticity gradient develops closer to the vortex axis, between 220 and 320 km radius (Fig. 6, lower left panel). However a linear stability analysis of the mean tangential wind profile in the middle layer at 60 h shows that it is not appreciably more unstable than at the initial time. Thus barotropic instability alone would not account for the rapid emergence of the azimuthal wavenumber-2 structure. In fact, a calculation of a 'no physics' version of the model initialized with the initial barotropic vortex together with its unstable wavenumber-2 eigenmode shows that the numerical diffusion in the model is sufficient to prevent growth of this eigenmode.

It is beyond the scope of this work to investigate the linear stability of the *evolving* baroclinic vortex in the model, but on the basis of the foregoing (but admittedly incomplete) stability analyses, we hypothesize that the growth of both asymmetries in the model is not a manifestation of dynamic instability and is most likely a consequence of the numerical approximation in the equations as suggested by ZSU. This hypothesis finds support in recent calculations by the third author, which show that the asymmetries are sensitive also to the type of vertical grid used in the model. The details of these calculations will be submitted for publication in due course.

6. Summary and conclusions

A two-dimensional version of the minimal three-dimensional tropical cyclone model of Zhu *et al.* has been used to examine certain basic aspects of tropical cyclone evolution. Comparison of the three-dimensional and axisymmetric versions of the model have been used to assess the importance of asymmetries on the dynamics of tropical cyclones. Vortex evolution is similar in the two models during the gestation period, although, for the same horizontal grid size, the latter is shorter in the axisymmetric model because of the higher effective resolution of the staggered grid. During the period of rapid intensification, the three-dimensional model develops marked asymmetries so that the maximum of the azimuthally-averaged tangential wind speed is significantly less than the maximum tangential wind speed in the two-dimensional calculation. The development of the asymmetries has a marked effect on the "pressure-wind relationship": typically minimum pressures are higher when asymmetries are present, although maximum wind speeds are similar in strength.

We examined the development of a region of supergradient winds in the surface boundary layer of the model cyclone. The calculations show that supergradient winds are to be expected because air parcels suffer large inward displacements in the boundary layer. Even though absolute angular momentum is only partially conserved in this layer, large tangential wind speeds that can be attained can exceed those that occur above the boundary layer, especially inside the radius of maximum tangential wind speed of the latter.

Stability indices indicate that regions of flow develop in the axisymmetric calculations, in which necessary conditions are met for inertial and barotropic instability. Mechanisms for the development of such regions are discussed. An analysis is presented that suggests why symmetric inertial stability is unlikely to materialize in a model with limited vertical resolution such as ours. We present evidence to support of the hypothesis that the asymmetries that develop in the three-dimensional version of the model are not a result of barotropic instability, but rather a consequence of the numerical approximations made.

Acknowledgement

We thank Harry Weber who carried out the stability analyses of the tangential wind profiles with the algorithm he developed some years ago. We are grateful also to Lloyd Shapiro and two anonymous referees for their comments on an earlier version of the manuscript. The first author was supported by a scholarship from the Australian International Development Programme (AusAid). The work was supported by the US Office of Naval Research Marine Meteorology Program through Grant No. N00014-95-1-0394.

References

Anthes, R. A., S. L. Rosenthal, and J. W. trout 1971a Preliminary results from an asymmetries model of a tropical cyclone. *Mon. Wea. Rev.*, **99,** 744-758

Anthes, R. A., J. W. Trout, and S. L. Rosenthal 1971b Comparisons of tropical cyclone simulations with and with the assumption of circular symmetry. *Mon. Wea. Rev.*, **99,** 759-766

Anthes, R. A. 1972 Development of asymmetries in a three-dimensional numerical model of a tropical cyclone. *Mon. Wea. Rev.*, **100,** 461-476

Anthes, R. A. 1974 The dynamics and energetics of mature tropical cyclones. *Rev. Geophys. Space Phys.*, **12,** 495-522

Arakawa, A. 1969 Parameterization of cumulus convection. *Proc. WMO/IUGG Symp. Numerical Weather Prediction, Tokyo, 26 November - 4 December 1968, Japan Meteor. Agency IV*, **8,** 1-6

Callaghan, J., and R. K. Smith 1998 The relationship between maximum surface wind speeds and central pressure in tropical cyclones. *Aust. Meteor. Mag.*, **47,** 191-202

DeMaria, M., and J. D. Pickle 1988 A simplified system of equations for simulating tropical cyclones. *J. Atmos. Sci.*, **45,** 1542-1554

Dengler, K. 1998 The effects of convection and baroclinicity on the motion of tropical-cyclone-like vortices. *Quart. J. Roy. Meteor. Soc.*, **124,** 699-727

Dengler, K., and M. J. Reeder 1997 The effects of convection and baroclinicity on the motion of tropical-cyclone-like vortices. *Quart. J. Roy. Meteor. Soc.*, **123,** 699-727

Dengler, K., and R. K. Smith 1998 A monsoon depression over northwestern Australia. Part II: A numerical model study. *Aust. Met. Mag.*, **47,** 135-144

Emanuel, K. A. 1986 An air-sea interaction theory for tropical cyclones. Part I: Steady-state maintenance. *J. Atmos. Sci.*, **43,** 585-604

Emanuel, K. A. 1989 The finite-amplitude nature of tropical cyclogenesis. *J. Atmos. Sci.*, **46,** 3431-3456

Emanuel, K. A. 1995 The behaviour of a simple hurricane model using a convective scheme based on subcloud-layer entropy equilibrium. *J. Atmos. Sci.*, **52,** 3960-3968

Emanuel, K. A. 1997 Some aspects of hurricane inner core dynamics and thermodynamics. *J. Atmos. Sci.*, **54,** 1014-1026

Flatau, M., and D. E. Stevens 1989 Barotropic and inertial instabilities in the hurricane outflow layer. *Geophys. Astrophys. Fluid Dyn.*, **47,** 1-18

Hack, J. J., and W. H. Schubert 1981 Nonlinear response of atmospheric vortices to heating by organized convection. *J. Atmos. Sci.*, **43,** 1559-1573

Jones, C. W., and E. J. Watson 1963 Two-dimensional boundary layers. Chapter 5 of *Laminar boundary layers. (Ed. L. Rosenhead) Clarendon Press, Oxford*, 687pp

Kepert, J. and Y. Wang 2001 The dynamics of boundary layer jets within the tropical cyclone core. Part II: Nonlinear enhancement. *J. Atmos. Sci.*, **58,** in press

Kurihara, Y. and R. E. Tuleya 1974 Structure of a tropical cyclone developed in a three-dimensional numerical simulation model. *J. Atmos. Sci.,* **31,** 893-919

Kossin, J. P., W. H. Schubert and M. T. Montgomery 2001 Unstable interactions between a hurricane's primary eyewall and a secondary ring of enhanced vorticity. *J. Atmos. Sci.*, **57,** 3893-3917

Rayleigh, Lord 1916 On the dynamics of revolving fluids. *Proc. Roy. Soc.*, **A, 93,** 148-154

Möller, J. D., and R. K. Smith 1994 The development of potential vorticity in a hurricane-like vortex. *Quart. J. Roy. Meteor. Soc.,* **120,** 1255-1265

Möller, J. D., and M. T. Montgomery 2000 Hurricane evolution via PV asymmetries in a three-dimensional asymmetric model. *J. Atmos. Sci.*, **57,** 3366-3387

Ooyama, K. V. 1969 Numerical simulation of the life cycle of tropical cyclones. *J. Atmos. Sci.*, **26,** 3-40

Ooyama, K. V. 1982 Conceptual evolution of the theory and modeling of the tropical cyclone. *J. Meteor. Soc. Japan*, **60,** 369-380

Ooyama, K. V. 1987 Numerical experiments of steady and transient jets with a simple model of the hurricane outflow layer. *Preprint volume, Seventeenth Conference on Tropical Meteor., Miami, FL*, 318-320

Reasor, P. D., M. T. Montgomery, F. D. Marks, and J. F. Gamarche 2000 Low-wavenumber structure and evolution of the hurricane inner core observed by dual-Doppler radar. *Mon. Wea. Rev.*, **128,** 1653-1680

Rosenthal, S. L.	1969	Preliminary results from numerical experiments a primitive equation model designed to simulate the motion of tropical cyclones. *Proc. WMO/IUGG Symp. Numerical Weather Prediction, Tokyo, 26 November - 4 December 1968, Japan Meteor. Agency*, **8,** 49-59
Rosenthal, S. L.	1970	A circularly-symmetric primitive equation model of tropical cyclone development containing an explicit water-vapour cycle. *Mon. Wea. Rev.*, **98,** 106-120
Rosenthal, S. L.	1971	The response of a tropical-cyclone model to variations in boundary-layer parameters, initial conditions, lateral boundary conditions, and domain size. *Mon. Wea. Rev.*, **99,** 767-777
Schubert W. H., and J. J. Hack	1982	Inertial stability and tropical cyclone development. *J. Atmos. Sci.*, **39,** 1687-1697
Schubert W. H., and B. T. Alworth	1987	Evolution of potential vorticity in tropical cyclones. *Quart. J. Roy. Meteor. Soc.*, **113,** 147-162
Schubert W. H., M. T. Montgomery, R. H. Taft, T. A. Guinn, S. R. Fulton, J. P. Kossin, and J. P. Edwards	1999	Polygonal eyewalls, asymmetric eye contraction, and potential vorticity mixing in hurricanes. *J. Atmos. Sci.*, **56,** 1197-1223
Shapiro, L. J.	1983	The asymmetric boundary layer under a translating hurricane. *J. Atmos. Sci.*, **40**, 1984-1998
Shapiro, L. J.	1992	Hurricane vortex motion and evolution in a three-layer model. *J. Atmos. Sci.*, **49**, 140-153
Shapiro, L. J.	2000	Potential vorticity asymmetries and tropical cyclone evolution in a three-layer model. *J. Atmos. Sci.*, **57**, 3645-3662
Smith, R. K.	1968	The surface boundary layer of a hurricane. *Tellus*, **20**, 473-483
Smith, R. K.	2000	The role of cumulus convection in hurricanes and its representation in hurricane models. *Rev. Geophys.,* **38,** 465-489
Smith, R. K.	2002	A simple model of the hurricane boundary layer. Submitted to *Quart. J. Roy. Meteor. Soc.* **128**
Snow, J. T.	1982	A review of recent advances in tornado vortex dynamics. *Rev. Geophys. Space Phys.* **20**, 953-964
Sundqvist, H.	1970	Numerical simulations of the development of tropical cyclones with a ten- level model. Part I. *Tellus*, **22,** 359-390
Wada, M.	1979	Numerical experiments of the tropical cyclone model by use of the Arakawa-Schubert parameterization. *J. Meteor. Soc. Japan*, **57,** 505-530
Weber, H., and R. K. Smith	1994	The stability of barotropic vortices: implications for tropical cyclone motion. *Geophys. Astrophys. Fluid Dyn.*, **70,** 1-30
Willoughby, H. E.	1995	Mature structure and motion. Chapter 2 of A global view of tropical cyclones. (Ed. R. L. Elsberry), World Meteorological Organization, Geneva, COMPLETE, pp21-62
Yamasaki, M.	1968a	Numerical simulation of tropical-cyclone development with the use of primitive equations. *J. Meteor. Soc. Japan,* **46,** 178-213
Yamasaki, M.	1968b	A tropical-cyclone model with parameterized vertical partition of released latent heat. *J. Meteor. Soc. Japan,* **46,** 202-214
Yamasaki, M.	1968c	Detailed analysis of a tropical-cyclone simulated with a 13-layer model. *Papers in Meteorology and Geophysics,* **20,** 559-585
Zhu, H., R. K. Smith and W. Ulrich	2001	A minimal three-dimensional tropical-cyclone model. *J. Atmos. Sci.*, **58,** 1924-1944

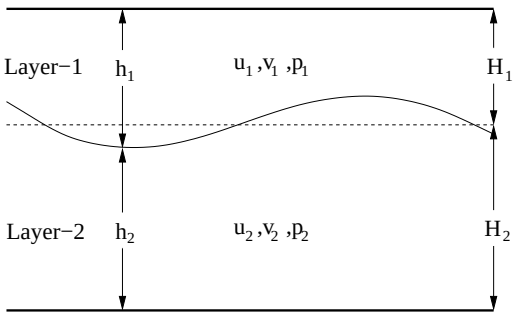

Figure A.1. Configuration of a two-layer model for illustrating inertial instability. See text for discussion.

Appendix

Inertial instability in a two-layer slab symmetric model

Consider the stability of a two-layer meridional shear flow on an f-plane in a slab-symmetric model as illustrated in Fig. 1. The upper and lower layers have uniform densities ρ_1 and ρ_2, depths h_1 and h_2, and mean depths H_1 and H_2, respectively, where $h_1 + h_2 = H_1 + H_2$ is a constant. Suppose there is an meridional flow $V_1(x)$ in the upper layer and $V_2(x)$ in the lower layer. The linearized equations of motion take the form

$$\frac{\partial u_n}{\partial t} - f v_n = -\frac{1}{\overline{\rho}} \frac{\partial p_n}{\partial x} \tag{A.1}$$

$$\frac{\partial v_n}{\partial t} + (\frac{dV_n}{dx} + f) u_n = 0 \tag{A.2}$$

$$\frac{\partial h_n}{\partial t} + H_n \frac{\partial u_n}{\partial x} = 0 \tag{A.3}$$

where u_n, v_n are the perturbation velocities and $n = 1, 2$. The hydrostatic equation relates $\partial p_2/\partial x$ to $\partial p_1/\partial x$, i.e.

$$\frac{\partial p_2}{\partial x} = \frac{\partial p_1}{\partial x} + g(\rho_2 - \rho_1) \frac{\partial h_2}{\partial x}, . \tag{A.4}$$

If dV_1/dx and dV_2/dx are both constants, the equations have perturbation wave solutions of the form

$$(u_n, v_n, p_n/\overline{\rho}, h_n - H_n) = (\hat{u}_n, \hat{v}_n, \hat{P}_n, \hat{h}_n) e^{i(kx - \omega t)}, \tag{A.5}$$

where k and ω and the qualities $(\hat{u}_n, \hat{v}_n, \hat{P}_n, \hat{h}_n)$, $(n = 1, 2)$, are constants. Substitution of (A6) into (A1)-(A5) leads to a set of eight homogeneous algebraic equations for the eight constants $\hat{u}_n$ etc. These equations have a nontrivial solution only if

$$\omega^2 = c_{IG}^2 k^2 + f(f + d\overline{V}/dx) \tag{A.6}$$

where $c_{IG} = [g(\rho_2 - \rho_1)/(\rho_1/H_1 + \rho_2/H_2)]^{1/2}$ is the phase-speed for long internal gravity waves and $d\overline{V}_n/dx = [(\rho_1/H_1)dV_1/dx + (\rho_2/H_2)dV_2/dx]/(\rho_1/H_1 + \rho_2/H_2)$ is a depth-weighted average meridional vorticity. Instability occurs if $\omega^2 < 0$, requiring that the depth-weighted absolute vorticity, $f + d\overline{V}/dx < 0$. Then inertial instability occurs for the wavenumbers k such that

$$k^2 < -\frac{f(f + d\overline{V}/dx)}{c_{IG}^2} = k_I^2, \text{ say.} \tag{A.7}$$

The foregoing analysis becomes more complicated if dV_1/dx and/or dV_2/dx vary with x. Then we may only substitute

$$(u_n, v_n, p_n/\overline{\rho}, h_n - H_n) = (\hat{u}_n(x), \hat{v}_n(x), \hat{P}_n(x), \hat{h}_n(x)) e^{-\omega t}, \tag{A.8}$$

and the x-dependence of waves has to be determined as part of the eigenvalue problem, which, in general, will have to be solved numerically. The same is true in the case of a vortex in cylindrical coordinates for a general swirling velocity. Nevertheless, the simple analysis described above allows a number of important inferences may be made:

1. Only waves of wavelength larger than $2\pi/k_I$ are unstable. Therefore the horizontal extent of the region over which $f + \overline{V}_x$ is negative is less than $2\pi/k_I$, instability will not occur.
2. The threshold wavelength for instability increases with increasing density contrast (i.e. static stability) in which case c_{IG} increases.
3. One may surmise that in a multi-layer or continuous system, waves of higher vertical wavenumber i.e. smaller phase speed will have a greater chance of being unstable at a given horizontal scale.
4. The existence of instability means that for some distributions of variables, lateral displacement on fluid parcels leads to forces in the same direction.

While these results are not quantitatively applicable to an axisymmetric vortex similar qualitative results may be expected in that case, but the mathematics will be more complicated.

Subgrid-scale diffusion

Some control of small-scale noise is achieved by the use of a third-order upwind advection scheme. Remaining spurious *small amplitude* two-grid-scale disturbances arising from the discretization of the equations are controlled here with a biharmonic damping term appended to all prognostic equations except the pressure tendency equation of the form

$$-k_4 \nabla^4 \chi,$$

where χ is any of the variables u, v, θ, q. The factor k_4 is a constant for a given resolution and is converted into a time and length scale with $k_4 = \Delta^4/\tau_4$. Here we use $\tau_4 = 6$ h. This damping is not sufficient to smear out the *large amplitude* shocks that arise at grid points where there is a sudden release of latent heat associated with explicit precipitation. For this reason we add a diffusion term to the right-hand-side of all prognostic equations (except for pressure): i.e.

$$K\nabla^2\chi - \delta_{[u,v],\chi}\frac{\chi}{r^2}$$

where $\delta_{[u,v],\chi} = 1$ for either $\chi = u$ or $\chi = v$, and $\delta_{[u,v],\chi} = 0$ otherwise. This procedure is formally equivalent to the representation of Reynolds stress terms in terms of an eddy diffusivity. The factor K is set proportional to the divergence, a procedure implemented by Ooyama (1984), i.e.

$$K = \left|\frac{1}{r}\frac{\partial(ru)}{\partial r}\right|\frac{\Delta}{\tau_2},$$

with $\tau_2 = 24$ h. The task of controlling the small-scale noise could be achieved with this filter also by specifying some minimum threshold for K. However, it is known that ∇^2 damping is less specific in damping short waves and may reduce the amplitudes of resolved modes to a higher degree than the biharmonic filter. This may cause an undesirable high overall diffusion, leading here, for example, to a retardation in the onset of rapid vortex intensification.

It should be stressed that the applied damping techniques have an effect on the outer boundary condition. The extra diffusion acts like a sponge for large amplitude gravity waves and reduces the amplitude of the waves that leave the computational domain. We have implemented a combination of a sponge and an open radiation boundary, which we found to be superior to a radiation boundary solely or a sponge solely in keeping reflections small, but this improvement is not a necessary ingredient to the present model. Hack and Schubert (1981) investigated pure radiation boundary conditions suitable for axisymmetric vortices at the outer radial boundary in a model without moisture and without extra damping. They stated that the some radiation boundary conditions they tested were suitable, but not perfect. They speculated that in a model with moisture included, the latent heat release might generate outward propagating gravity waves with larger amplitudes than in their model. We applied an extra Newtonian damping in the outermost quarter of the domain up to the maximum radius R where the radiation condition is applied to reduce the amplitude of such gravity waves, so that the imperfections of the radiation boundary condition are less critical. Specifically we add Newtonian damping terms of the form $-\nu u$ and $-\nu v$ to the momentum equations for u and v in outermost quarter of the domain in order to diminish the amplitude of disturbances that may reach the outer boundary. The damping coefficient increases with radius according to

$$\nu = \frac{1}{2\tau_1}\left(1 - \cos\left(\frac{(r - r_d)\pi}{R - r_d}\right)\right)$$

where r_d is the radius at which the Newtonian damping is first applied and $\tau_1 = 360$ s.